

Frame-wise Motion and Appearance for Real-time Multiple Object Tracking

Jimuyang Zhang¹

zhangjim@andrew.cmu.edu

Sanping Zhou²

sanpingzhou@stu.xjtu.edu.cn

Jinjun Wang²

jinjun@mail.xjtu.edu.cn

Dong Huang¹

donghuang@cmu.edu

¹ The Robotics Institute,

Carnegie Mellon University,
Pittsburgh, USA

² Artificial Intelligence and Robotics,

Xi'an Jiaotong University,
Xi'an, China

Abstract

The main challenge of Multiple Object Tracking (MOT) is the efficiency in associating indefinite number of objects between video frames. Standard motion estimators used in tracking, e.g., Long Short Term Memory (LSTM), only deal with single object, while Re-Identification (Re-ID) based approaches exhaustively compare object appearances. Both approaches are computationally costly when they are scaled to a large number of objects, making it very difficult for real-time MOT. To address these problems, we propose a highly efficient Deep Neural Network (DNN) that simultaneously models association among indefinite number of objects. The inference computation of the DNN does not increase with the number of objects. Our approach, Frame-wise Motion and Appearance (FMA), computes the Frame-wise Motion Fields (FMF) between two frames, which leads to very fast and reliable matching among a large number of object bounding boxes. As auxiliary information is used to fix uncertain matches, Frame-wise Appearance Features (FAF) are learned in parallel with FMFs. Extensive experiments on the MOT17 benchmark show that our method achieved real-time MOT with competitive results as the state-of-the-art approaches.¹

1 Introduction

The goal of Multiple Object Tracking (MOT) is to jointly estimate the trajectories of all interested object targets in videos [63, 51, 56, 52]. MOT has been a critical perception technique required in many real-time applications such as autonomous driving [6], field robotic [40] and video surveillance [59].

With the significant achievements made in object detection [29, 57, 58], the tracking by detection framework has been popularized in the past few years. Given the object detection results in each frame, this line of tracking methods aim to associate the same objects across different frames. Typically, the object association problem is solved in two steps: (1) Solving a bipartite matching problem between the objects detected in two frames; (2) Optimizing

this solution to find one-to-one matches using the Hungarian algorithm [22]. In order to achieve high tracking performance, the energy function of bipartite matching is often very computationally costly to solve. As a consequence, the resulting MOT algorithm can hardly be real-time in practical computing platforms, *e.g.*, desktop computing nodes, embedded CPU/GPU modules, and FPGA.

The situation becomes even worse when the powerful yet computation hungry Deep Neural Networks (DNN) are used for MOT. DNNs significantly outperform the classical approaches in estimating motion patterns and extracting discriminate appearance features. However, existing DNNs specialized for these tasks cannot be directly used to achieve efficient MOT: (1) These DNNs usually contain heavy back-bone networks for feature extraction from images, such as the ResNet [18] and GoogleNet [47]; (2) The off-the-shelf Re-Identification (Re-ID) models [7, 44, 59] compute discriminative features independently for each object bounding box, which is very costly when scaling-up to multiple objects; (3) The DNNs that learn object associations [45] need to pre-set the number of objects as a part of the fixed network structure, which cannot handle indefinite number of objects in practice. (4) Time-consuming post-processing algorithms are used to deduce the final association results given appearance and motion patterns [48] produced by DNNs. As a result, many DNN approaches for MOT do not consider real-time scenarios.

In this paper, we achieve real-time MOT by using a highly efficient deep learning approach, called Frame-wise Motion and Appearance (FMA). Our DNN learns (1) Frame-wise Motion Fields (FMF), a novel association representation that simultaneously accommodates indefinite number of objects. (2) Frame-wise Appearance Feature (FAF), the holistic discriminative appearance features for Re-ID. Specifically, the pixel-wise responses in FMFs are the coordinate shifts of bounding boxes between two sequential frames. FMFs allow us to use very simple operations to shift bounding boxes and find the corrected matches in both frames. FAFs are learned over all objects of each frame under the Re-ID loss. In inference, they only need to be cropped for a few objects where FMFs are uncertain with one-to-one matches. Besides, we present a simple yet effective inference algorithm to associate object bounding boxes into trajectories. With unoptimized Pytorch (Float32) implementation on a PC with single TitanXP GPU, our FMA has achieved 25FPS on the MOT17 benchmark videos with comparable performance to state-of-the-art algorithms. The main contributions of this work can be highlighted as follows:

- Frame-wise Motion Fields (FMF) to represent the association among indefinite number of objects between frames.
- Frame-wise Appearance Feature (FAF) to provide Re-ID features to assist FMF-based object association.
- A simple yet effective inference algorithm to link the objects according to FMFs, and to fix a few uncertain associations using FAFs.
- Experiments on the challenging MOT17 benchmark show that our method achieves real-time MOT with competitive performance as the state-of-the-art approaches.

2 Related Work

Because our method jointly learns the motion patterns and appearance features for MOT, we briefly review these two lines of MOT methods, *i.e.*, motion models and appearance models,

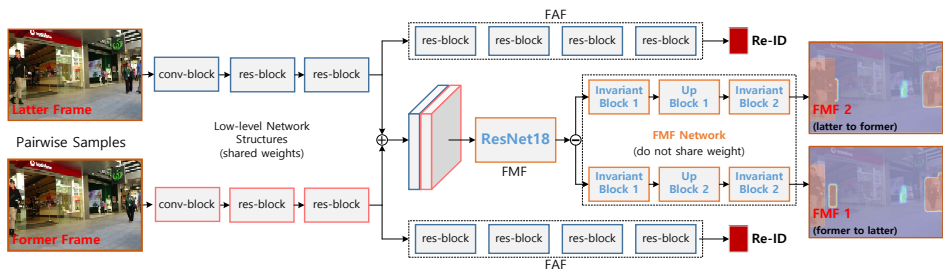


Figure 1: DNN architecture of our FMA approach. The DNN takes two frames as input and produces the Frame-wise Motion Fields (FMF) and Frame-wise Re-ID Features (FAF). FMF simultaneously models the motion of multiple objects, while FAFs provide appearance cues in case FMFs fail to associate certain objects.

in the following paragraphs.

Motion Model. The motion models describe how each target moves from frame to frame, which is the key of MOT to locate the search regions of a target in the next frame. Existing motion models can be roughly divided into linear and nonlinear cases. The linear methods [32, 34, 50] assume objects move with constant velocity across frames, while the nonlinear methods [10, 34] model inconstant velocities. In the earlier works, the Kalman filter [19] has been widely used to estimate motion in most MOT methods [2, 9, 20]. With the blooming of DNNs, a large number of deep learning based methods have been designed to learn the motion patterns. For example, the Long Short Term Memory (LSTM) networks [21, 33, 42, 55] model can describe and predict complex motion patterns of a target over multiple frames. Both the Kalman filter and LSTM based models belong to the nonlinear methods, therefore they are robust in handling occlusions in the long-term tracking. Due to the strong modeling capability of DNN, the deep motion based methods [42, 50] have achieved the state-of-the-art results on the public benchmark datasets. However, these motion models only take the object locations as input, therefore can not explore any appearance or contextual information to help predict the objects positions. Our FMFs are motion representations estimated from appearance and contextual information of the video frames.

Appearance Model. The appearance models produce discriminative features of objects in all frames, such that features of the same object are more similar than those of different objects. In earlier tracking approaches, the color histogram [9, 24, 26, 49] and pixel-based template representations [35, 33] are standard hand-crafted features used to describe the appearance of objects. In addition to using Euclidean distances to measure appearance similarity, the covariance matrix representation was also applied to compare the pixel-wise similarities, such as the SIFT-like features [17, 51] and pose features [36, 40]. In recent years, the deep feature learning based methods have been popularized with the blooming of DNNs. For example, the features of multiple convolution layers are explored to enhance the discriminative capability of learned features [8]. In [4], an online feature learning model is designed to associate both the detection results and short tracklets. Moreover, different network structures, such as siamese network [25], triplet network [39] and quadruplet network [44], have been extensively used to learn the discriminative features from the detected object bounding boxes. Benefitting from the powerful representation capability of deep features, this line of methods [11, 5, 14, 45] have achieved the state-of-the-art results on the public benchmark datasets. However, most approaches compute discriminative features independently for each object bounding box, which is very costly when scaling-up to multiple objects. Our FAF

Invariant Block 1 ($p = 1$)	Up Block ($s = 2$)	Invariant Block 2 ($p = 1$)
$Conv(3 \times 3, 512, 512)$	$Decomv(3 \times 3, 512, 256) + ReLU$	$Conv(3 \times 3, 320, 128)$
$BN + ReLU$	$Decomv(3 \times 3, 512, 256) + ReLU$	$BN + ReLU$
$Conv(3 \times 3, 512, 512)$	$Decomv(3 \times 3, 384, 256) + ReLU$	$Conv(3 \times 3, 128, 64)$
$BN + ReLU$	$Decomv(3 \times 3, 320, 256) + ReLU$	$BN + ReLU$
		$Conv(3 \times 3, 64, 2)$

Table 1: The detailed structure of FMF network, in which ‘Conv’ means the normal convolution layer, ‘BN’ denotes the batch normalization layer, ‘ReLU’ indicates the rectified linear unit, ‘Deconv’ means the normal deconvolution layer, and p, s are the striding and padding parameters, respectively.

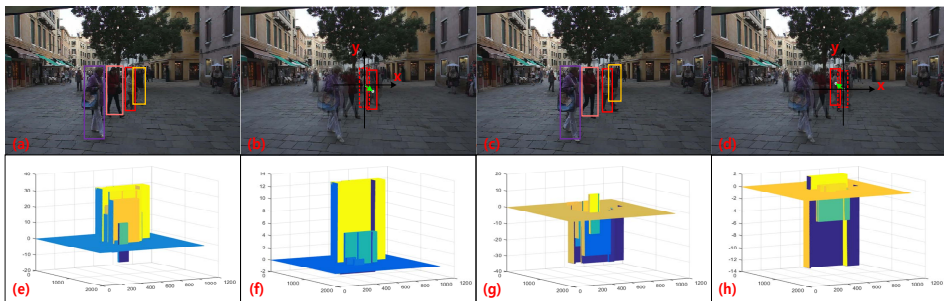


Figure 2: Visualization of the FMFs produced on two input frames, in which the colored bounding boxes contain the objects to be tracked. Specifically, (a) and (c) denote two input frames, (b) and (d) illustrate how to decompose the FMFs to horizontal and vertical directions for frame (a) and (c), respectively. The second row visualizes the computed FMFs, in which (e) and (f) represent the horizontal and vertical FMFs for frame (a), while (g) and (h) represent the horizontal and vertical FMFs for frame (c).

learning is conducted on the frame basis and multiple objects are handled simultaneously.

3 Our Method (FMA)

Our MOT method consists of a DNN (Figure 1) and an inference algorithm. Candidate objects to be tracked are pre-detected in each frame using the image-based object detectors. For instance, the MOT challenges² provide object candidates detected by DPM [13], FR-CNN [68] and SDP [12]. Our DNN takes two frames as input and produces the Frame-wise Motion Fields (FMFs) and Frame-wise Re-ID Features (FAFs). The inference algorithm uses FMFs to associate objects between the two frames and uses FAFs to fix associations where FMFs fail. Both the DNN and inference algorithm are very efficient, making it possible for real-time MOT. The DNN consists of conv-blocks and res-blocks of the same structure as [62]. Detailed structure of our FMF network is summarized in Table 1.

3.1 Frame-wise Motion Fields

Denote the two input frames as the former frame $\mathbf{I}_1 \in \mathbb{R}^{w \times h \times 3}$ and the latter frame $\mathbf{I}_2 \in \mathbb{R}^{w \times h \times 3}$. Besides, b_i denotes the bounding box of the i -th object to be associated between the two frames. The x and y coordinates of b_i in two frames are $\mathcal{X}_1(b_i)$, $\mathcal{X}_2(b_i)$ and $\mathcal{Y}_1(b_i)$,

² <https://motchallenge.net/>

$\mathcal{Y}_2(b_i)$, respectively. The DNN (Figure 1) produces four FMFs that represent the motion between frame \mathbf{I}_1 and frame \mathbf{I}_2 . Formally, the ground truth of FMFs is computed as:

$$\mathbf{F}_x^1(b_i) = \mathcal{X}_2(b_i) - \mathcal{X}_1(b_i), \mathbf{F}_y^1(b_i) = \mathcal{Y}_2(b_i) - \mathcal{Y}_1(b_i), \quad (1)$$

$$\mathbf{F}_x^2(b_i) = \mathcal{X}_1(b_i) - \mathcal{X}_2(b_i), \mathbf{F}_y^2(b_i) = \mathcal{Y}_1(b_i) - \mathcal{Y}_2(b_i), \quad (2)$$

where $\mathbf{F}_x^1(b_i) \in \mathfrak{R}^{w \times h \times 1}$ and $\mathbf{F}_y^1(b_i) \in \mathfrak{R}^{w \times h \times 1}$ contains the motion vectors of bounding box b_i assigned on the pixels in \mathbf{I}_1 . Similarly, $\mathbf{F}_x^2(b_i)$, $\mathbf{F}_y^2(b_i)$ contains the motion vectors of bounding box b_i assigned on the pixels in \mathbf{I}_2 . In Figure 2, we visualize the FMFs on two input frames. Note that we chose to predict the bi-directional motion vectors of b_i between \mathbf{I}_1 and \mathbf{I}_2 , respectively. This design enforces robust estimation of motion vectors: since b_i in former and latter frames usually contain different appearance and contextual information, they can help each other in estimating motions. Moreover, it also deals with two cases in inference: *Case (1)* certain b_i exists in \mathbf{I}_1 but disappears in \mathbf{I}_2 , and *Case (2)* certain b_i is not in \mathbf{I}_1 but appears in \mathbf{I}_2 . In our later inference algorithm, $\mathbf{F}_x^1(b_i)$ and $\mathbf{F}_y^1(b_i)$ are used to associate the detections from the former to latter frame, while $\mathbf{F}_x^2(b_i)$ and $\mathbf{F}_y^2(b_i)$ are used to associate the detections from the later to former frame.

The FMFs simultaneously embed multiple object affinity information and can be directly learned by the network in an end-to-end manner. To learn the FMFs, we simply use the Mean Square Error (MSE) as the loss function:

$$\mathcal{L}_{MSE} = \sum_{k=1}^2 \sum_{b_i \in \mathbf{B}} \|\mathbf{H}_x^k(b_i) - \mathbf{F}_x^k(b_i)\|_F^2 + \|\mathbf{H}_y^k(b_i) - \mathbf{F}_y^k(b_i)\|_F^2, \quad (3)$$

where \mathbf{H}_y^k and \mathbf{H}_x^k are the outputs of network on the former and latter frames, and \mathbf{B} is the set of all the object bounding boxes to be associated.

3.2 Frame-wise Appearance Features

Our FMFs can successfully solve association for most objects in benchmark database, but there are still some extreme cases. For instance, when frames are noisy and objects are crowded, FMFs may not be estimated perfectly for every objects between two frames. As a practical extension for extreme cases, our MOT approach finds several candidate bounding boxes according to FMFs, and uses the re-identification (Re-ID) approach to verify the identity of an object among these candidates.

The standard Re-ID approaches [46, 59] mainly focus on generating powerful appearance representation to associate the same object captured from difference cameras and far-away time lapses. They take image patches of each object bounding box and use a specialized DNNs to learn discriminative features from these image patches. Given the powerful FMFs, we found that learning decent Re-ID features only requires a few convolutions. Moreover, to achieve fast MOT, we avoid using an independent DNN for Re-ID feature learning by jointly computing the Re-ID features with FMFs. We also keep the DNN inference computation invariant to the number of objects by learning frame-wise features. As shown in Fig. 1, our DNN learns FAFs in parallel with FMFs.

Given the bounding boxes of objects in two frames, our Re-ID step crops patches from FAFs and computes the similarity between two cropped features. In training, the cropped features of the same objects are concatenated as the positive samples, and that of different objects are concatenated as negative samples. In practice, the number of negative and positive

samples are kept as 4 : 1. FMFs are learned by training on the Binary Cross-Entropy (BCE) loss:

$$\mathcal{L}_{BCE} = -\frac{1}{N} \sum_{j=1}^N \mathcal{S}_j \log h(\mathbf{p}_j) + (1 - \mathcal{S}_j) \log(1 - h(\mathbf{p}_j)) \quad (4)$$

where \mathbf{p}_j is the j th sample, \mathcal{S}_j denotes the class label of \mathbf{p}_j , in which $\mathcal{S}_j = 0$ means \mathbf{p}_j contains features from the same object, otherwise $\mathcal{S}_j = 1$.

3.3 Inference Algorithm

Given FMFs and FAFs, our inference algorithm efficiently associates the detection results between frames, and produces the track for each detected object.

Formally, $\mathbf{D} = \{\mathbf{D}_1, \dots, \mathbf{D}_N\}$ denotes the detection results, *e.g.*, object bounding boxes, in N videos frames. $\mathbf{T} = \{\mathbf{T}^1, \dots, \mathbf{T}^M\}$ denotes the tracks of M objects. $\text{IOU}(\cdot)$ is the operator to compute the bounding box overlap between the last detection of an active track and candidate detections in the next frame, and $\text{SIM}(\cdot)$ measures the appearance similarities between the last detection of an active track and candidate detections in the next frame. Our inference algorithm conducts MOT in three steps, **Step 1**: Associate the tracks from the former to latter frame; **Step 2**: Associate the tracks from the later to former frame; **Step 3**: Associate the remaining tracks and detections with FAFs. For simplicity, we use \mathbf{T}_A , \mathbf{T}_B , \mathbf{T}_C , \mathbf{T}_D to store the unmatched tracks after each step. The detailed inference process is summarized in Algorithm 1. The algorithm does not need to solve any optimization problem or learn any parameters. We only introduce two thresholds τ_1 (IOU threshold) and τ_2 (Re-ID similarity threshold) to help decide the association process.

4 Experiments

4.1 Dataset and Setting

Dataset. We conducted experiments on the MOT17 dataset, which is the latest benchmark for multiple human tracking. This dataset contains various challenging video sequences recorded by static or moving cameras, and under the complex scenes of illumination changes, varying viewpoints and weather conditions. In total, there are 7 fully annotated training videos and 7 testing videos, in which public detection results are obtained by three image-based object detectors: DPM [13], FRCNN [68] and SDP [14].

Setting. In the training process, the input frame-pairs were composed under two intervals: two frames every 1 frame, and every 4 frames. The training batch size is 4, the learning rate is initialized to be 0.001 and decreased by a factor of 0.1 at 70 epochs. In the testing process, the input frame-pairs are taken under as two frames every 1 frame. The inference hardware is a PC with an Intel Xeon(R) 3.80GHz CPU, 64GB RAM, and a NVIDIA GTX TitanXP GPU. The DNN was implemented in Pytorch under Float32 and the inference algorithm in Python without parallel speedup. We set $\tau_1 = 0.45$ and $\tau_2 = 0.5$ for all the testing videos.

4.2 Ablation Study

In this section, we analyze our method from two aspects: MOT result of each component and effectiveness of FMFs.

Algorithm 1 Inference algorithm based on FMFs and FAFs for real-time MOT

```

1: Input: Initial detections:  $\mathbf{D} = \{\mathbf{D}_i\}_{i=1}^N$ , final FMF model:  $\mathbf{H}$  and Re-ID model  $\mathbf{P}$ .
2: Parameter:  $\tau_1$  (IOU threshold) and  $\tau_2$  (Re-ID similarity threshold).
3: Output: Final tracks:  $\mathbf{T} = \{\mathbf{T}^k\}_{k=1}^M$ , where  $\mathbf{T}^k = \{\mathbf{t}_i^k\}_{i=1}^N$ .
4: Initialize the tracks  $\mathbf{T}$  using  $\mathbf{D}_1$ ;
5: for  $i = 1; i < N; i++$  do
6:   Initialize the track  $\mathbf{T}_A, \mathbf{T}_B, \mathbf{T}_C$  and  $\mathbf{T}_D$  using  $\mathbf{T}, a = 0$  and  $b = 0$ ;
7:   for  $k = 1; k \leq \|\mathbf{T}_A^i\|; k++$  do
8:     Compute the IOU score:  $\mathbf{d}_{i+1}^k, \mathbf{s}_{i+1}^k = \text{IOU}(\mathbf{H}_{1,2}(\mathbf{T}_A^{i,k}), \mathbf{D}_{i+1})$ ;
9:     Find the candidates:  $\mathbf{s}_c = \text{SORT}(\mathbf{s}_{i+1}^k > \tau_1)$ 
10:    if  $\|\mathbf{s}_c\| = 1$  then
11:      Update  $\mathbf{t}_i^k$  by adding  $\mathbf{d}_{i+1}^k(1), \mathbf{D}_{i+1}$  by deleting  $\mathbf{d}_{i+1}^k(1), \mathbf{T}_B^i, \mathbf{T}_C^i$  and  $\mathbf{T}_D^i$  by deleting  $\mathbf{t}_i^k$ ;
12:       $++a$ ;
13:    else
14:      Compute the appearance score:  $d_{i+1}^k, c_{i+1}^k = \max\{\text{SIM}(\mathbf{P}(\mathbf{T}_A^{i,k}), \mathbf{P}(\mathbf{D}_{i+1}))\}$ ;
15:      if  $c_{i+1}^k > \tau_2$  then
16:        Update  $\mathbf{t}_i^k$  by adding  $d_{i+1}^k, \mathbf{D}_{i+1}$  by deleting  $d_{i+1}^k, \mathbf{T}_B^i, \mathbf{T}_C^i$  and  $\mathbf{T}_D^i$  by deleting  $\mathbf{t}_i^k$ ;
17:         $++a$ ;
18:      else
19:        Update  $\mathbf{t}_i^k$  by adding  $\mathbf{d}_{i+1}^k(1), \mathbf{D}_{i+1}$  by deleting  $\mathbf{d}_{i+1}^k(1), \mathbf{T}_B^i, \mathbf{T}_C^i$  and  $\mathbf{T}_D^i$  by deleting  $\mathbf{t}_i^k$ ;
20:         $++a$ ;
21:      end if
22:    end if
23:  end for
24:  for  $k = 1; k \leq \|\mathbf{T}_B^i\|; k++$  do
25:    Compute the IOU score:  $\mathbf{d}_{i+1}^{k+a}, \mathbf{s}_{i+1}^{k+a} = \text{IOU}(\mathbf{H}_{3,4}(\mathbf{D}_{i+1}), \mathbf{T}_B^{i,k+a})$ ;
26:    Find the candidates:  $\mathbf{s}_c = \text{SORT}(\mathbf{s}_{i+1}^{k+a} > \tau_1)$ 
27:    if  $\|\mathbf{s}_c\| = 1$  then
28:      Update  $\mathbf{t}_i^{k+a}$  by adding  $\mathbf{d}_{i+1}^{k+a}(1), \mathbf{D}_{i+1}$  by deleting  $\mathbf{d}_{i+1}^{k+a}(1), \mathbf{T}_C^i$  and  $\mathbf{T}_D^i$  by deleting  $\mathbf{t}_i^{k+a}$ ;
29:       $++b$ ;
30:    else
31:      Compute the appearance score:  $d_{i+1}^{k+a}, c_{i+1}^{k+a} = \max\{\text{SIM}(\mathbf{P}(\mathbf{T}_B^{i,k+a}), \mathbf{P}(\mathbf{D}_{i+1}))\}$ ;
32:      if  $c_{i+1}^{k+a} > \tau_2$  then
33:        Update  $\mathbf{t}_i^{k+a}$  by adding  $d_{i+1}^{k+a}, \mathbf{D}_{i+1}$  by deleting  $d_{i+1}^{k+a}, \mathbf{T}_C^i$  and  $\mathbf{T}_D^i$  by deleting  $\mathbf{t}_i^{k+a}$ ;
34:         $++b$ ;
35:      else
36:        Update  $\mathbf{t}_i^{k+a}$  by adding  $\mathbf{d}_{i+1}^{k+a}(1), \mathbf{D}_{i+1}$  by deleting  $\mathbf{d}_{i+1}^{k+a}(1), \mathbf{T}_C^i$  and  $\mathbf{T}_D^i$  by deleting  $\mathbf{t}_i^{k+a}$ ;
37:         $++b$ ;
38:      end if
39:    end if
40:  end for
41:  for  $k = 1; k \leq \|\mathbf{T}_C^i\|; k++$  do
42:    Compute the appearance score:  $d_{i+1}^{k+a+b}, c_{i+1}^{k+a+b} = \max\{\text{SIM}(\mathbf{P}(\mathbf{T}_C^{i,k+a+b}), \mathbf{P}(\mathbf{D}_{i+1}))\}$ ;
43:    if  $c_{i+1}^{k+a+b} > \tau_2$  then
44:      Update  $\mathbf{t}_i^{k+a+b}$  by adding  $d_{i+1}^{k+a+b}, \mathbf{D}_{i+1}$  by deleting  $d_{i+1}^{k+a+b}$ , and  $\mathbf{T}_D^i$  by deleting  $\mathbf{t}_i^{k+a+b}$ ;
45:    end if
46:  end for
47:  Initialize the rest of  $\mathbf{D}_{i+1}$  as new targets and terminate the targets in  $\mathbf{T}_D^i$ .
48: end for

```

MOT result of each component. Our DNN jointly learns FMFs and FAFs for MOT. We show in Table 2 that when conducting inference using only FMFs or FAFs, the performances are close to each other but very different in speed. FMFs can effectively associate the detections between two frames, resulting in very fast MOT at 27.5 Hz. Without FMFs, inference with only FAFs need to conduct Re-ID on every pair of candidate bounding boxes,

Methods	MOTA \uparrow	MT \uparrow	ML \downarrow	FP \downarrow	FN \downarrow	ID \downarrow	Frag \downarrow	Hz \uparrow
FMF	56.3	21.5%	33.2%	4,961	74,754	2,539	3,141	27.5
FAF	57.3	23.8%	30.6%	6,632	71,707	2,012	5,083	5.3
FMA (FMF+FAF)	57.5	24.1%	30.2%	6,655	71,720	1,553	4,899	25.2

Table 2: Results achieved by each component of our method on the MOT17 benchmark.

Methods	MOTA \uparrow	MOTP \uparrow	MT \uparrow	ML \downarrow	FP \downarrow	FN \downarrow	ID \downarrow	Frag \downarrow	Hz \uparrow
PHD	48.0	77.2	17.1%	35.6%	23,199	265,954	3,998	8,886	6.7
EAMTT	42.6	76.0	12.7%	42.7%	30,711	288,474	4,488	5,720	1.4
GMPHD	39.6	74.5	8.8%	43.3%	50,903	284,228	5,811	7,414	3.3
GM_PHD	36.4	74.5	4.1%	57.3%	23,723	330,767	4,607	11,317	38.4
MTDF	49.6	75.5	18.9%	33.1%	37,124	241,768	5,567	9,260	1.2
MOTDT	50.9	76.6	17.5%	35.7%	24,069	250,768	2,474	5,317	18.3
FMA	47.4	76.6	17.1%	35.8%	21,498	271,237	4,019	13,107	25.2

Table 3: Comparisons with state-of-the-art online methods on the MOT17 benchmark. MOT metrics were computed over all three object detectors provided by MOT17.



Figure 3: The predicted bounding boxes (yellow) by FMFs between two adjacent frames. The blue and magenta boxes are the bounding boxes provided by the SDP object detectors.

leading to a much slower speed at 5.3 Hz. In FMA (FMF+FAF), FMFs can find high-quality matches for most objects, and FAFs were only used to handle the remaining hard cases. As a result, FMA shows good trade-off between speed and accuracy.

Effectiveness of FMFs. FMFs contain pixel-wise estimation of displacement between the detected bounding boxes in adjacent frames: a former frame and a latter frame. From FMFs, our algorithm computes the displacement for each bounding box, and produces a prediction of each bounding box in both the former and latter frame. The one-to-one matching between the predicted bounding box and the detected bounding box is simply found by computing IOU. Figure 3 shows that our approach can effectively deal with the complex motion patterns in the tracking process. The first row and the second row are the former and the latter frames, respectively. The predicted bounding boxes are plotted in yellow, and the bounding boxes in the former and latter frame are plotted in blue and magenta, respectively. The high IOUs between the predicted and detected bounding boxes indicate that the learned FMFs can successfully associate the detections between two adjacent frames.

4.3 Comparison

In this section, we compare our method with other state-of-the-art online methods on the MOT17 challenge benchmark. The compared methods include the MOTDT [80], PHD [15], EAMTT [43], GMPHD [23], GM_PHD [10], MTDF [16] models, in which the MOTDT is a deep learning based method and the others are based on traditional approaches.

The results are shown in Table 3, from which we can conclude that: (1) The deep learning based methods usually outperform the traditional methods in accuracy. (2) Our method

Detectors	Methods	MOTA \uparrow	MT \uparrow	ML \downarrow	FP \downarrow	FN \downarrow	ID \downarrow	Frag \downarrow
DPM [13]	MOTDT	46.5%	14.6%	40.5%	8,841	90,990	802	1,860
	MTDF	44.5%	13.6%	39.0%	11,822	90,539	1,999	3,371
	FMA	39.6%	10.8%	43.7%	5,409	106,965	1,276	5,065
FRCNN [68]	MOTDT	47.7%	15.4%	35.9%	8,911	88,773	731	1,540
	MTDF	47.2%	18.7%	31.8%	15,119	82,331	1,804	2,937
	FMA	45.1%	16.3%	33.6%	9,434	92,552	1,190	3,143
SDP [14]	MOTDT	58.4%	22.5%	30.7%	6,317	71,005	941	1,917
	MTDF	57.0%	24.2%	28.4%	10,183	68,898	1,764	2,952
	FMA	57.5%	24.1%	30.2%	6,655	71,720	1,553	4,899

Table 4: Comparisons of MOT methods with individual detectors on the MOT17 benchmark.



Figure 4: Challenging tracking examples by FMA with the SDP detector. Different targets are marked by different colors and numbers.

has achieved a faster speed while performs a bit worse in overall accuracy than MOTDT. **Note that**, FMA achieved 25FPS with unoptimized Pytorch (Float32) implementation on a PC with single-TitanXP GPU. The above performance was achieved only by training from scratch on the MOT17 data.

The reason for the lower overall accuracy of our approach comes from two aspects: (1) Unlike MOTDT that used external person Re-ID datasets (*i.e.*, CUHK01 [27], CUHK03 [28], Market1501 [68]), our method was only trained on MOT17 data and did not use any external data to enhance FAFs; (2) Our method favors strong detection results, because accurate FMFs and FAFs need to be learned from scratch in training. In Table 4, we show MOT performance using three different detector results provided by MOT17. Here we compare our method with two best-performing models, *i.e.*, MOTDT and MTDF. We can see that our method achieves very competitive results when the FRCNN and SDP detectors were used.

Moreover, we show some tracking examples by our method on four challenging video sequences in Figure 4. Our method is robust to illumination changes, varying viewpoints and mutual occlusion. Nevertheless, in challenging videos, it is not easy to get accurate frame-based object detection results. In the future, we plan to further relief the reliance on strong detectors by training FMFs on short video clips instead of two frames. This will make FMF robust to outliers in the frame-wise detection results.

5 Conclusion

Practical and real-time MOT has to scale well with indefinite number of objects. This paper addresses this problem with frame-wise representations of object motion and appearance. In particular, FMFs simultaneously handle forward and backward motions of all bounding boxes in two input frames, which is the key to achieve real-time MOT inference. FAFs helps FMFs in handling some hard cases without significantly compromising the speed. The FMFs and FAFs are efficiently used in our inference algorithm, and achieved faster and more competitive results on the MOT17 benchmark. Our frame-wise representations are very efficient and general, making it possible to achieve real-time inference on more computationally expensive tracking tasks, such as instance segmentation tracking and scene mapping.

References

- [1] Multi-object tracking using online metric learning with long short-term memory. In *ICIP*, pages 788–792. IEEE, 2018.
- [2] Anton Andriyenko and Konrad Schindler. Multi-target tracking by continuous energy minimization. In *CVPR*, pages 1265–1272. IEEE, 2011.
- [3] Anton Andriyenko, Konrad Schindler, and Stefan Roth. Discrete-continuous optimization for multi-target tracking. In *CVPR*, pages 1926–1933. IEEE, 2012.
- [4] Seung-Hwan Bae and Kuk-Jin Yoon. Confidence-based data association and discriminative deep appearance learning for robust online multi-object tracking. *TPAMI*, 40(3):595–610, 2018.
- [5] Lucas Beyer, Stefan Breuers, Vitaly Kurin, and Bastian Leibe. Towards a principled integration of multi-camera re-identification and tracking through optimal bayes filters. In *CVPR Workshops*, pages 29–38, 2017.
- [6] Chenyi Chen, Ari Seff, Alain Kornhauser, and Jianxiong Xiao. Deepdriving: Learning affordance for direct perception in autonomous driving. In *ICCV*, pages 2722–2730, 2015.
- [7] Dapeng Chen, Dan Xu, Hongsheng Li, Nicu Sebe, and Xiaogang Wang. Group consistent similarity learning via deep crf for person re-identification. In *CVPR*, pages 8649–8658, 2018.
- [8] Long Chen, Haizhou Ai, Chong Shang, Zijie Zhuang, and Bo Bai. Online multi-object tracking with convolutional neural networks. In *ICIP*, pages 645–649. IEEE, 2017.
- [9] Wongun Choi and Silvio Savarese. Multiple target tracking in world coordinate with single, minimally calibrated camera. In *ECCV*, pages 553–567. Springer, 2010.
- [10] Caglayan Dicle, Octavia I Camps, and Mario Sznaiar. The way they move: Tracking multiple targets with similar appearance. In *ICCV*, pages 2304–2311, 2013.
- [11] Volker Eiselein, Daniel Arp, Michael Pätzold, and Thomas Sikora. Real-time multi-human tracking using a probability hypothesis density filter and multiple detectors. In *2012 IEEE Ninth International Conference on Advanced Video and Signal-Based Surveillance*, pages 325–330. IEEE, 2012.
- [12] Andreas Ess, Bastian Leibe, and Luc Van Gool. Depth and appearance for mobile scene analysis. In *ICCV*, pages 1–8. IEEE, 2007.
- [13] Pedro F Felzenszwalb, Ross B Girshick, David McAllester, and Deva Ramanan. Object detection with discriminatively trained part-based models. *TPAMI*, 32(9):1627–1645, 2010.

- [14] Tharindu Fernando, Simon Denman, Sridha Sridharan, and Clinton Fookes. Tracking by prediction: A deep generative model for mutli-person localisation and tracking. In *WACV*, pages 1122–1132. IEEE, 2018.
- [15] Zeyu Fu, Pengming Feng, Federico Angelini, Jonathon Chambers, and Syed Mohsen Naqvi. Particle phd filter based multiple human tracking using online group-structured dictionary learning. *IEEE Access*, 6:14764–14778, 2018.
- [16] Zeyu Fu, Federico Angelini, Jonathon Chambers, and Syed Mohsen Naqvi. Multi-level cooperative fusion of gm-phd filters for online multiple human tracking. *TMM*, 2019.
- [17] Brian Fulkerson, Andrea Vedaldi, and Stefano Soatto. Localizing objects with smart dictionaries. In *ECCV*, pages 179–192. Springer, 2008.
- [18] Kaiming He, Xiangyu Zhang, Shaoqing Ren, and Jian Sun. Deep residual learning for image recognition. In *CVPR*, pages 770–778, 2016.
- [19] Rudolph Emil Kalman. A new approach to linear filtering and prediction problems. *Journal of basic Engineering*, 82(1):35–45, 1960.
- [20] Ahmed T Kamal, Jawadul H Bappy, Jay A Farrell, and Amit K Roy-Chowdhury. Distributed multi-target tracking and data association in vision networks. *TPAMI*, 38(7):1397–1410, 2016.
- [21] Chanho Kim, Fuxin Li, and James M Rehg. Multi-object tracking with neural gating using bilinear lstm. In *ECCV*, pages 200–215, 2018.
- [22] Harold W Kuhn. The hungarian method for the assignment problem. *Naval research logistics quarterly*, 2(1-2):83–97, 1955.
- [23] Tino Kutschbach, Erik Bochinski, Volker Eiselein, and Thomas Sikora. Sequential sensor fusion combining probability hypothesis density and kernelized correlation filters for multi-object tracking in video data. In *AVSS*, pages 1–5. IEEE, 2017.
- [24] Nam Le, Alexander Heili, and Jean-Marc Odobez. Long-term time-sensitive costs for crf-based tracking by detection. In *ECCV*, pages 43–51. Springer, 2016.
- [25] Laura Leal-Taixé, Cristian Canton-Ferrer, and Konrad Schindler. Learning by tracking: Siamese cnn for robust target association. In *CVPR Workshops*, pages 33–40, 2016.
- [26] Bastian Leibe, Konrad Schindler, Nico Cornelis, and Luc Van Gool. Coupled object detection and tracking from static cameras and moving vehicles. *TMAMI*, 30(10):1683–1698, 2008.
- [27] Wei Li, Rui Zhao, and Xiaogang Wang. Human reidentification with transferred metric learning. In *ACCV*, 2012.
- [28] Wei Li, Rui Zhao, Tong Xiao, and Xiaogang Wang. Deepreid: Deep filter pairing neural network for person re-identification. In *CVPR*, 2014.
- [29] Wei Liu, Dragomir Anguelov, Dumitru Erhan, Christian Szegedy, Scott Reed, Cheng-Yang Fu, and Alexander C Berg. Ssd: Single shot multibox detector. In *ECCV*, pages 21–37. Springer, 2016.
- [30] Chen Long, Ai Haizhou, Zhuang Zijie, and Shang Chong. Real-time multiple people tracking with deeply learned candidate selection and person re-identification. In *ICME*, 2018.
- [31] David G Lowe. Distinctive image features from scale-invariant keypoints. *IJCV*, 60(2):91–110, 2004.

- [32] Anton Milan, Konrad Schindler, and Stefan Roth. Multi-target tracking by discrete-continuous energy minimization. *TPAMI*, 38(10):2054–2068, 2016.
- [33] Anton Milan, S Hamid Rezatofighi, Anthony Dick, Ian Reid, and Konrad Schindler. Online multi-target tracking using recurrent neural networks. In *AAAI*, 2017.
- [34] Shaul Oron, Aharon Bar-Hillel, and Shai Avidan. Extended lucas-kanade tracking. In *ECCV*, pages 142–156. Springer, 2014.
- [35] Stefano Pellegrini, Andreas Ess, Konrad Schindler, and Luc Van Gool. You’ll never walk alone: Modeling social behavior for multi-target tracking. In *ICCV*, pages 261–268. IEEE, 2009.
- [36] Zhen Qin and Christian R Shelton. Social grouping for multi-target tracking and head pose estimation in video. *TPAMI*, 38(10):2082–2095, 2016.
- [37] Joseph Redmon, Santosh Divvala, Ross Girshick, and Ali Farhadi. You only look once: Unified, real-time object detection. In *CVPR*, pages 779–788, 2016.
- [38] Shaoqing Ren, Kaiming He, Ross Girshick, and Jian Sun. Faster r-cnn: Towards real-time object detection with region proposal networks. In *NIPS*, pages 91–99, 2015.
- [39] Ergys Ristani and Carlo Tomasi. Features for multi-target multi-camera tracking and re-identification. In *Proceedings of the IEEE Conference on Computer Vision and Pattern Recognition*, pages 6036–6046, 2018.
- [40] Patrick Ross, Andrew English, David Ball, Ben Upcroft, and Peter Corke. Online novelty-based visual obstacle detection for field robotics. In *ICRA*, pages 3935–3940. IEEE, 2015.
- [41] Markus Roth, Martin Bäuml, Ram Nevatia, and Rainer Stiefelhagen. Robust multi-pose face tracking by multi-stage tracklet association. In *ICPR*, pages 1012–1016. IEEE, 2012.
- [42] Amir Sadeghian, Alexandre Alahi, and Silvio Savarese. Tracking the untrackable: Learning to track multiple cues with long-term dependencies. In *ICCV*, pages 300–311, 2017.
- [43] Ricardo Sanchez-Matilla, Fabio Poiesi, and Andrea Cavallaro. Online multi-target tracking with strong and weak detections. In *ECCV*, pages 84–99. Springer, 2016.
- [44] Jeany Son, Mooyeol Baek, Minsu Cho, and Bohyung Han. Multi-object tracking with quadruplet convolutional neural networks. In *ICCV*, pages 5620–5629, 2017.
- [45] ShiJie Sun, Naveed Akhtar, HuanSheng Song, Ajmal Mian, and Mubarak Shah. Deep affinity network for multiple object tracking. *arXiv preprint arXiv:1810.11780*, 2018.
- [46] Yifan Sun, Liang Zheng, Yi Yang, Qi Tian, and Shengjin Wang. Beyond part models: Person retrieval with refined part pooling (and a strong convolutional baseline). In *ECCV*, pages 480–496, 2018.
- [47] Christian Szegedy, Wei Liu, Yangqing Jia, Pierre Sermanet, Scott Reed, Dragomir Anguelov, Dumitru Erhan, Vincent Vanhoucke, and Andrew Rabinovich. Going deeper with convolutions. In *CVPR*, pages 1–9, 2015.
- [48] Siyu Tang, Mykhaylo Andriluka, Bjoern Andres, and Bernt Schiele. Multiple people tracking by lifted multicut and person re-identification. In *CVPR*, pages 3539–3548, 2017.
- [49] Rahul Rama Varior, Bing Shuai, Jiwen Lu, Dong Xu, and Gang Wang. A siamese long short-term memory architecture for human re-identification. In *ECCV*, pages 135–153. Springer, 2016.

- [50] Xingyu Wan, Jinjun Wang, and Sanping Zhou. An online and flexible multi-object tracking framework using long short-term memory. In *CVPR Workshops*, pages 1230–1238, 2018.
- [51] Shaofei Wang and Charless C Fowlkes. Learning optimal parameters for multi-target tracking. In *BMVC*, volume 1, page 6, 2015.
- [52] Nicolai Wojke, Alex Bewley, and Dietrich Paulus. Simple online and realtime tracking with a deep association metric. In *ICIP*, pages 3645–3649. IEEE, 2017.
- [53] Zheng Wu, Ashwin Thangali, Stan Sclaroff, and Margrit Betke. Coupling detection and data association for multiple object tracking. In *CVPR*, pages 1948–1955. IEEE, 2012.
- [54] Bo Yang and Ram Nevatia. An online learned crf model for multi-target tracking. In *CVPR*, pages 2034–2041. IEEE, 2012.
- [55] Tianyu Yang and Antoni B Chan. Recurrent filter learning for visual tracking. In *ICCV*, pages 2010–2019, 2017.
- [56] Young-chul Yoon, Abhijeet Boragule, Young-min Song, Kwangjin Yoon, and Moongu Jeon. Online multi-object tracking with historical appearance matching and scene adaptive detection filtering. In *AVSS*, pages 1–6. IEEE, 2018.
- [57] Shun Zhang, Jinjun Wang, Zelun Wang, Yihong Gong, and Yuehu Liu. Multi-target tracking by learning local-to-global trajectory models. *Pattern Recognition*, 48(2):580–590, 2015.
- [58] Liang Zheng, Liyue Shen, Lu Tian, Shengjin Wang, Jingdong Wang, and Qi Tian. Scalable person re-identification: A benchmark. In *ICCV*, 2015.
- [59] Sanping Zhou, Jinjun Wang, Jiayun Wang, Yihong Gong, and Nanning Zheng. Point to set similarity based deep feature learning for person re-identification. In *CVPR*, pages 3741–3750, 2017.
- [60] Ji Zhu, Hua Yang, Nian Liu, Minyoung Kim, Wenjun Zhang, and Ming-Hsuan Yang. Online multi-object tracking with dual matching attention networks. In *ECCV*, pages 366–382, 2018.